
NUMERICAL SOLUTION OF THE L^1 -OPTIMAL TRANSPORT PROBLEM ON SURFACES

Luca Bertini

CNRS
Université de Strasbourg,
Strasbourg, France
berti@math.unistra.fr

Enrico Facca

Centro Ennio de Giorgi,
Scuola Normale Superiore,
Pisa, Italy
enrico.facca@sns.it

Mario Putti

Department of Mathematics “Tullio Levi-Civita”
University of Padova
Padova, Italy
putti@math.unipd.it

ABSTRACT

In this article we study the numerical solution of the L^1 -Optimal Transport Problem on 2D surfaces embedded in \mathbb{R}^3 , via the DMK formulation introduced in [1]. We extend from the Euclidean into the Riemannian setting the DMK model and conjecture the equivalence with the solution Monge-Kantorovich equations, a PDE-based formulation of the L^1 -Optimal Transport Problem. We generalize the numerical method proposed in [1, 2] to 2D surfaces embedded in \mathbb{R}^3 using the Surface Finite Element Model approach to approximate the Laplace-Beltrami equation arising from the model. We test the accuracy and efficiency of the proposed numerical scheme, comparing our approximate solution with respect to an exact solution on a 2D sphere. The results show that the numerical scheme is efficient, robust, and more accurate with respect to other numerical schemes presented in the literature for the solution of L^1 -Optimal Transport Problem on 2D surfaces.

Keywords Monge-Kantorovich equations · Optimal Transport · Numerical Solution · Wasserstein Distance · Riemannian Manifolds · Triangulated Surfaces

1 Introduction

The *Optimal Transport Problem* (OT problem), first introduced by Monge in [3] and reformulated by Kantorovich in [4], looks for the optimal strategy to re-allocate a resource from one place (X) to another (Y) for a given unit-mass transportation cost $c(x, y)$ ($x \in X$, $y \in Y$), typically chosen as $c(x, y) = |x - y|^p$. This problem captured the attention of a number of authors (extensive reviews can be found in [5, 6, 7, 8]), and, prompted by the fluid dynamic interpretation of the quadratic cost problem proposed in [9, 10], a number of mathematical and numerical formulations of the OT problem have been proposed in different fields of applications [11, 12, 13, 14, 15].

For $p = 1$, i.e., the cost is linear with respect to the distance, $c(x, y) = |x - y|$, the problem is named L^1 Optimal Transport (L^1 -OT problem), and is exactly the problem originally posed by Monge [3]. In this case, the non-strict convexity of the cost makes the mathematical analysis more complicated and increases the difficulties of its numerical solution. On the other hand, this problem, and the related problem of calculating the Wasserstein-1 distance, seems to be more robust with respect to noise distances defined with other cost functions (e.g., the quadratic cost $p = 2$) [16]. The L^1 problem can be reformulated in several equivalent ways (see [5] for a complete overview), which can be exploited in the quest for efficient numerical solvers.

Various numerical methods exploiting these different formulations of the (L^1 -OT problem) have been developed in recent years [17, 18], but the subject is still a very active field of research. Among the most widely used numerical solution methods, we can name the Sinkhorn approach described in [19] and its variants [16]. These methods are based on entropy regularization, i.e., they solve a relaxed version of the linear programming problem associated to the Kantorovich formulation of the OT problem, and have been successfully applied in many different fields, such as computer graphics [15] or machine learning [20]. One of their limitations is that they are not suitable for transported densities that are sums of Dirac measures [20].

Recently, [1] introduced a dynamic reformulation of the Monge-Kantorovich equations (MK equations), the PDE-based form of the (L^1 -OT problem) proposed by [21]. The authors conjecture that the solution of the MK equations is exactly the long-time limit of a system of differential equations, called the Dynamic Monge-Kantorovich (DMK), that couples a diffusion PDE with an ODE describing the dynamics of the diffusion coefficient. Unfortunately, a complete proof of the conjecture is still missing. However, some theoretical results reported in [1, 2] and extensive numerical evidence presented in [2] strongly support the claim that MK equations can be solved via the DMK approach. More recently, [22] have shown that the equilibrium of a slight modification of a relaxed version of the DMK indeed converges in a weak sense to the solution of the MK equations, providing additional support to the above conjecture. The DMK formulation can be easily solved numerically using standard methods and provides an efficient numerical approach not only for the solution of two- and three-dimensional L^1 -OT problems, but also for the calculation of the Wasserstein-1 distance between measures [2].

The L^1 -OT problem can be naturally extended from the Euclidean setting to a Riemannian manifold $M \subset \mathbb{R}^n$ with metric g by simply replacing the Euclidean distance with the geodesic distance as the transport cost [23, 24]. However, this extension poses non-trivial numerical challenges, in primis the computation of the geodesic distance itself. Recent numerical discretizations of OT problems on discrete surfaces can be found in [25, 15, 26, 27].

In the present paper, we extend the DMK model proposed in [1] to the Riemannian setting. We ambient the DMK model on a manifold M with a Riemannian metric g and address in particular the case in which either f^- or f^+ or both are continuous with respect to the volume form. The extension of the DMK to Riemannian manifolds is obtained via an appropriate substitution of the relevant differential operators with geometry-based equivalents, and takes inspiration from the definitions introduced in [24]. Next, we adapt the numerical methods proposed in [2] to solve the DMK on two-dimensional surfaces embedded in \mathbb{R}^3 . The DMK equations are discretized in time by means of explicit Euler time stepping and in space by means of the Surface Finite Element technique developed in [28]. Mimicking the approach used in the Euclidean (planar) case, the spatial discretization is obtained by a combination of piecewise constant and conforming piecewise linear basis functions on nested grids to satisfy a sort of inf-sup stability condition. The resulting approach has the same computational properties and costs of the planar \mathbb{R}^2 equivalent, and thus provides a very efficient tool for the numerical solution of OT problem on surfaces.

The convergence properties of the developed algorithm are verified on a test case defined on the unit sphere for which a closed form solution of the MK equations is developed starting from the results reported in [29]. We experimentally show the convergence towards steady state of the proposed dynamics and evaluate the experimental convergence rates of the spatial approximation, convergence in the approximation of the Wasserstein-1 distance between two measures is tested and is found experimentally to be more than quadratic with respect to the mesh parameter h .

Finally, the results obtained with our proposed approach are compared with those obtained using the method proposed in [25]. This method, tailored to the calculation of the L^1 -OT problem, also called Earth's Mover Distance (EMD), is based on the solution of Beckmann problem, which can be shown to be equivalent to the L^1 -OT problem [8]. Beckmann problem tries to minimize the L^1 -norm of the vector-valued measure v subject to the constraint that its divergence must be equal to the difference between the transported densities. The method proposed in [25], which we denote with EMDADMM, approximates the minimizer of Beckmann problem by means of the Alternating Direction Method of Multipliers in combination with a clever FEM discretization of the divergence constraint. Our experimental results show that the DMK approach is more accurate being characterized by a faster convergence rate both in the approximation of the minimizer of the L^1 -OT problem and in the computation of the Wasserstein-1 distance.

The paper is organized as follows. After a short introduction of the different formulations of the Euclidean L^1 -OT problem of interest for our developments, we summarize the needed variations when the ambient space is a Riemannian manifold, with particular emphasis to the DMK approach. Then, we describe the extension of the numerical formulation of the DMK from the Euclidean to the Riemannian setting and how surface-FEM can be effectively developed to obtain the proposed numerical formulation of the L^1 -OT problem. Finally, the numerical tests are presented.

2 The L^1 optimal transportation problem

2.1 The Kantorovich problem

The Kantorovich formulation of the L^1 -OT problem in the Euclidean setting can be given as follows. Consider a convex and compact subset $\Omega \subset \mathbb{R}^d$ with smooth boundary and let $|x - y|$ be the Euclidean distance between two points x and y in \mathbb{R}^d . Denote with $\mathcal{M}_+(\Omega)$ the set of non-negative Radon measures supported in Ω . Given two finite

measures $f^+, f^- \in \mathcal{M}_+(\Omega)$ such that $f^+(\Omega) = f^-(\Omega)$, find the optimal plan γ^* belonging to the set

$$\Pi(f^+, f^-, \Omega) = \left\{ \gamma \in \mathcal{M}_+(\Omega \times \Omega) : \begin{array}{l} \text{for all } A, B \text{ Borel sets of } \Omega \\ \gamma(A, \Omega) = f^+(A) \quad \gamma(\Omega, B) = f^-(B) \end{array} \right\} \quad (1)$$

that solves the following minimization problem:

$$\inf_{\gamma} \left\{ \int_{\Omega \times \Omega} |x - y| d\gamma(x, y) : \gamma \in \Pi(f^+, f^-, \Omega) \right\}. \quad (2)$$

The resulting infimum defines a distance $W_1(f^+, f^-)$ between f^+ and f^- , which is called the Wasserstein-1 or Kantorovich-Rubinstein distance.

2.2 The MK equations

The above problem can be rewritten in many different forms (see e.g. [5]). Here we are interested in the PDE formulation, called *Monge-Kantorovich equations* (MK equations), introduced in [21]. We present these equations as formulated in [30]. Denoting with $\text{Lip}_1(\Omega)$ the space of continuous functions with Lipschitz constant equal to 1, we look for the pair $(u^*, \mu^*) \in (\text{Lip}_1(\Omega), \mathcal{M}_+(\Omega))$ that satisfies the following nonlinear system of PDEs:

$$-\text{div}_{\mu}(\mu \nabla_{\mu} u) = f^+ - f^- \quad \text{on } \Omega \quad (3a)$$

$$|\nabla_{\mu} u| \leq 1 \quad \text{on } \Omega \quad (3b)$$

$$|\nabla_{\mu} u| = 1 \quad \mu - a.e. \text{ in } \Omega, \quad (3c)$$

where ∇_{μ} denotes the gradient with respect to the measure μ as described in [31, 32]. Note that eq. (3a) must be interpreted in the following weak form:

$$\int_{\Omega} \nabla_{\mu} u(x) \cdot \nabla_{\mu} \phi(x) d\mu(x) = \int_{\Omega} \phi(x) df^+(x) - \int_{\Omega} \phi(x) df^-(x) \quad \forall \phi \in \mathcal{C}^1(\Omega), \quad (4)$$

which implies zero Neumann boundary conditions and must be complemented by the constraint that u has zero average. The components of the solution pair (u^*, μ^*) of the above system are named Kantorovich potential and OT density. Among the several results available on the MK equations, we recall here the few that will be used in this work (see, e.g., [33, 5, 34, 35]). Specifically, if either one of the measures f^+ and f^- admits a density with respect to the Lebesgue measure, then μ^* admits a unique density with respect to the Lebesgue measure. Moreover, when μ^* admits a density the notion of gradient ∇_{μ} with respect to a measure coincides with the notion of Sobolev weak gradient (see [31, Example 2.3, Appendix]). It is important to remark that there exist infinitely many functions u^* that satisfy eq. (3). In fact outside $\text{supp}(\mu^*)$ it is possible to perturb any solution u^* and still satisfy all constraints of eq. (3). However, in the support of μ^* the Kantorovich potential is unique [21].

2.3 The Beckmann Problem

The MK equations are related also to another equivalent formulation of the L^1 -OT problem, called *Beckmann Problem* (see [8]). The latter problem tries to find the optimal vector-valued measure $v \in [\mathcal{M}(\Omega)]^d$ that solves the following minimization problem:

$$\min_{v \in [\mathcal{M}(\Omega)]^d} \int_{\Omega} |dv| : \text{div}(v) = f^+ - f^-, \quad (5)$$

where $|dv|$ denotes the total variation measure of dv (see [8]). The MK equations and the Beckmann Problem are equivalent in the sense that v^* is related to μ^* and u^* by:

$$dv^* = -d\mu^* \nabla_{\mu^*} u^*. \quad (6)$$

Note that, when at least one of f^+ or f^- admits L^1 -density with respect to the Lebesgue measure, then $v^* = -\mu^* \nabla u^* \in [L^1(\Omega)]^d$ and problem eq. (5) can be rewritten as:

$$\min_{v \in [L^1(\Omega)]^d} \int_{\Omega} |v| dx : \text{div}(v) = f^+ - f^-.$$

2.4 The Dynamic Monge-Kantorovich equations

The model proposed in [1, 2] considers the case of either f^+ or f^- having L^2 -density with respect to the Lebesgue measure. With an abuse of notation, we will denote with f^+ and f^- both the measures and their densities. The model, named Dynamic Monge-Kantorovich (DMK) formulation (encapsulated here within a separate problem statement as it forms the basic starting point for our numerical developments), reads as follows.

Problem 1 (Dynamic Monge-Kantorovich (DMK) equations). *Consider a convex and bounded domain Ω in \mathbb{R}^d with smooth boundary and let $f^+, f^- : \Omega \rightarrow \mathbb{R}_{\geq 0}$ be such that $\int_{\Omega} f^+(x) dx = \int_{\Omega} f^-(x) dx$. Find the pair (μ, u) with $\mu : \mathbb{R}_{\geq 0} \times \Omega \mapsto \mathbb{R}_{\geq 0}$ and $u : \mathbb{R}_{\geq 0} \times \Omega \mapsto \mathbb{R}$ that satisfies:*

$$\begin{cases} -\operatorname{div}(\mu(t, x)\nabla u(t, x)) = f^+(x) - f^-(x) \\ \partial_t \mu(t, x) = \mu(t, x)(|\nabla u(t, x)| - 1) \\ \mu(0, x) = \mu_0(x) > 0. \end{cases} \quad (7)$$

with zero Neumann boundary conditions on $\partial\Omega$ and $\int_{\Omega} u = 0$.

In [1] the authors conjecture that the solution $(\mu(t, \cdot), u(t, \cdot))$ of Problem 1 is asymptotically equivalent to the solution (μ^*, u^*) of the MK equations eq. (3). In support of this conjecture, in [2] the authors propose a Lyapunov-candidate functional \mathcal{L} defined on non-negative densities $\bar{\mu} \in L^1(\Omega)$ and given by the sum of an energy and a mass functional, i.e.:

$$\mathcal{L}(\bar{\mu}) := \mathcal{E}(\bar{\mu}) + \mathcal{M}(\bar{\mu}) \quad (8)$$

$$\mathcal{E}(\bar{\mu}) := \sup_{\phi \in \operatorname{Lip}(\Omega)} \left\{ \int_{\Omega} \left((f^+ - f^-)\phi - \bar{\mu} \frac{|\nabla \phi|^2}{2} \right) dx \right\} \quad \mathcal{M}(\bar{\mu}) := \frac{1}{2} \int_{\Omega} \bar{\mu} dx. \quad (9)$$

The functional \mathcal{L} can be rewritten as:

$$\mathcal{L}(\bar{\mu}) = \frac{1}{2} \int_{\Omega} \bar{\mu} |\nabla \mathcal{U}(\bar{\mu})|^2 dx + \frac{1}{2} \int_{\Omega} \bar{\mu} dx$$

as long as the energy \mathcal{E} in eq. (9) admits a maximizer $\mathcal{U}(\bar{\mu})$ that is the weak solution of the PDE $-\operatorname{div}(\bar{\mu}\nabla \bar{u}) = f^+ - f^-$ with zero-Neumann boundary condition.

The main advantage of this formulation is that the introduction of the dynamics allows the implementation of efficient numerical algorithms for the solution of the original MK equations [2]. We summarize in the following Proposition the main results proved in [1, 2].

Proposition 1. *The OT density μ^* is the unique minimizer of \mathcal{L} and the corresponding infimum value is exactly the Wasserstein-1 distance between f^+ and f^- : $\mathcal{L}(\mu^*) = W_1(f^+, f^-)$. Moreover, for any $T > 0$ for which a solution pair $(\mu(t, \cdot), u(t, \cdot))$ of Problem 1 exists, for $t \in [0, T]$ the functional \mathcal{L} decreases along the μ -trajectory.*

More recently, in [22] the authors addressed a modified version of the DMK problem and were able to prove global existence of a time-asymptotic solution and its convergence (in a weak sense) toward the solution of the MK equations. The proof is based on the reformulation of the dynamical system in eq. (7) as a Gradient Flow in metric spaces [36] for the functional \mathcal{L} , contributing to strengthen the theoretical background of the original DMK model. On the other hand, experimental numerical results with this modified formulation show that it is not as efficient and robust as the original formulation proposed in [1, 2]. For this reason, we continue working in this paper with the latter.

2.5 Extension to manifolds

We restrict our discussion to the case of a compact manifold (M, g) (M for short) with no boundary and equipped with a smooth metric g . We denote with $\langle v, w \rangle_{g(x)}$ the application of the metric g evaluated at x to the two vectors $v, w \in T_x M$. Moreover we denote with ∇_g and $|\cdot|_g$ the gradient and the vector norm with respect to the metric tensor g . The distance induced by the metric g is defined as:

$$\operatorname{dist}_g(x, y) = \inf \left\{ \int_0^1 \sqrt{\langle \dot{\sigma}(s), \dot{\sigma}(s) \rangle_{g(\sigma(s))}} ds : \begin{array}{l} \sigma \in \mathcal{C}^1([0, 1], M) \\ \sigma(0) = x, \sigma(1) = y \end{array} \right\},$$

and we denote with dV_g the volume form induced by the metric g .

Now we can proceed with the formulation of the OT problem on a manifold (M, g) , adapting the notation and results of [24] to our setting. Replacing in eqs. (1) and (2) the domain Ω with M and the Euclidean distance term $|x - y|$ with

the distance $\text{dist}_g(x, y)$, the L^1 -OT problem on M tries to find the optimal plan $\gamma^* \in \Pi(f^+, f^-, M)$ that solves the minimization problem:

$$\inf_{\gamma} \left\{ \int_{M \times M} \text{dist}_g(x, y) d\gamma(x, y) : \gamma \in \Pi(f^+, f^-, M) \right\}.$$

This infimum value is exactly the Wasserstein-1 distance $W_{1,g}(f^+, f^-)$ on M . The Monge-Kantorovich equations described in eq. (3) can be generalized as well and become:

$$-\text{div}_{g,\mu}(\mu \nabla_{g,\mu} u) = f^+ - f^- \quad \text{on } M \quad (10a)$$

$$|\nabla_{g,\mu} u|_g \leq 1 \quad \text{on } M \quad (10b)$$

$$|\nabla_{g,\mu} u|_g = 1 \quad \mu - a.e. \quad (10c)$$

where eq. (10a) must be interpreted in the following weak form

$$\begin{aligned} \int_M \langle \nabla_{g,\mu} u(x), \nabla_{g,\mu} \phi(x) \rangle_{g(x)} d\mu(x) &= \\ &= \int_M \phi(x) df^+(x) - \int_M \phi(x) df^-(x) \quad \forall \phi \in C^1(M), \end{aligned} \quad (11)$$

where $\int_M u = 0$ is assumed. Likewise the Euclidean case, if μ^* admits a density with respect to the measure dV_g , the gradient $\nabla_{g,\mu}$ in eq. (10) coincides with the classical weak gradient ∇_g on M . Existence and uniqueness results of the OT density in a Riemannian setting were proved in [23], while L^p summability is still an open question.

Beckmann Problem (eq. (5)) can be transported as well into a manifold becoming:

$$\min_{v \in [M(M)]^n} \int_M |dv|_g : \text{div}_g(v) = f^+ - f^- \quad (12)$$

and eq. (6) holds also in this Riemannian setting. Again, when at least one of f^+ or f^- admits L^1 -density with respect to the volume form, eq. (12) can be rewritten as:

$$\min_{v \in [L^1(M)]^n} \int_M |v|_g dV_g : \text{div}_g(v) = f^+ - f^-,$$

where, similarly to eq. (6), the tangent velocity field is given by:

$$v^* = -\mu^* \nabla_g u^*. \quad (13)$$

Finally, we discuss next the extension of the DMK formulation from the Euclidean to the Riemannian setting. This is obtained by simply replacing the Euclidean differential operators with the Riemannian ones identified with the metric g as subscript. Thus we will write $|\cdot|_g$, $\langle \cdot, \cdot \rangle_g$, div_g , and ∇_g for $|\cdot|$, $\langle \cdot, \cdot \rangle$, div , and ∇ , respectively. Then, the Riemannian version of Problem 1 can be written as follows.

Problem 2 (Surface Continuous DMK). *Let (M, g) be a n -dimensional smooth compact manifold with no boundary and let $f^+, f^- \in L^2(M)$ be such that $\int_M f^+ dV_g = \int_M f^- dV_g$. Find the pair (μ, u) with $\mu : \mathbb{R}_{\geq 0} \times M \mapsto \mathbb{R}_{\geq 0}$ and $u : \mathbb{R}_{\geq 0} \times M \mapsto \mathbb{R}$ satisfying:*

$$\begin{cases} -\text{div}_g(\mu(t, x) \nabla_g u(t, x)) = f^+(x) - f^-(x) \\ \partial_t \mu(t, x) = \mu(t, x) (|\nabla_g u(t, x)| - 1) \\ \mu(0, x) = \mu_0(x) > 0, \end{cases} \quad (14)$$

with u having zero mean.

The generalization to the Riemannian setting of the Lyapunov-candidate functional in eq. (8) for any non-negative $\mu \in L^1(M)$ is also straightforward:

$$\begin{aligned} \mathcal{L}_g(\mu) &:= \mathcal{E}_g(\mu) + \mathcal{M}_g(\mu) \quad (15) \\ \mathcal{E}_g(\mu) &:= \sup_{\phi \in \text{Lip}(M)} \left\{ \int_M \left((f^+ - f^-) \phi - \mu \frac{|\nabla_g \phi|^2}{2} \right) dV_g \right\} \quad \mathcal{M}_g(\mu) := \frac{1}{2} \int_M \mu dV_g. \end{aligned}$$

It is immediate to show that, mutata mutandis, Proposition 1 holds also in this setting. It is thus natural to extend also the conjecture of the convergence of the solution of eq. (14) toward the solution of the MK equations in eq. (10).

3 Numerical Discretization

This section is dedicated to the development of the numerical discretization for Problem 2 obtained by extending to the surface setting the numerical DMK formulation proposed in [1, 2] for the Euclidean framework. The approach is based on the Method Of Lines (MOL) and considers a 2-dimensional compact surface Γ with no boundary, embedded in \mathbb{R}^3 . Eqs. (14) are first discretized in space and then the resulting ODE system is discretized in time. The long-time numerical solution of the latter is used to approximate the solution of the MK equations. We start by describing the (formal) weak formulation of the continuous surface DMK system obtained by exploiting the Hilbert space structure of $H^1(\Gamma)$ and $L^2(\Gamma)$. We test the system using functions in these spaces to yield:

$$\int_{\Gamma} \mu(t) \langle \nabla_g u(t), \nabla_g \psi \rangle_g dV_g = \int_{\Gamma} (f^+ - f^-) \psi dV_g, \quad \psi \in H^1(\Gamma) \quad (16a)$$

$$\int_{\Gamma} \partial_t \mu(t) \xi(x) dV_g = \int_{\Gamma} \mu(t) \left(|\nabla_g u(t)|_g - 1 \right) \xi dV_g, \quad \xi \in L^2(\Gamma) \quad (16b)$$

$$\int_{\Gamma} \mu(0) \xi dV_g = \int_{\Gamma} \mu_0 \xi dV_g \quad \xi \in L^2(\Gamma) \quad (16c)$$

$$\int_{\Gamma} u \psi dV_g = 0 \quad \xi \in H^1(\Gamma), \quad (16d)$$

ho aggiunto l'equazione per la media where, for simplicity, we have dropped the spatial dependence of the dependent variables.

3.1 Spatial discretization

Spatial discretization of eq. (7) follows the Surface Finite Element Method (SFEM) described in [28]. SFEM can be summarized in two steps: i) discretization of the surface and ii) definition of the finite dimensional FEM spaces. In the first step, we assume that the smooth surface Γ can be subdivided by a surface triangulation $\mathcal{T}(\Gamma)$ formed by the union of non-intersecting surface geodesic elements (triangles) $\mathbb{E}_i \in \Gamma$, $i = 1, \dots, N_{\mathbb{E}}$. Thus, similarly to the flat case, we have that $\Gamma = \mathcal{T}(\Gamma) = \cup_{i=1}^{N_{\mathbb{E}}} \mathbb{E}_i$ and $\sigma_{ij} = \mathbb{E}_i \cap \mathbb{E}_j$ is a geodesic curve on Γ connecting triangle vertices i and j . This triangulation is then approximated by its piecewise linear interpolant $\mathcal{T}_h(\Gamma) = \Gamma_h$, where Γ_h is defined by the union of 2-simplices in \mathbb{R}^3 (flat three-dimensional triangles) having the same vertices of $\mathcal{T}(\Gamma)$. The triangulation $\mathcal{T}_h(\Gamma)$ is assumed to be closely inscribed in the sense of [37], or equivalently, in the sense of [28]. Thus, we require that $\mathcal{T}_h(\Gamma) \subset \mathcal{N}_\epsilon$, where $\mathcal{N}_\epsilon \supset \Gamma$ is a tubular neighborhood of Γ of radius ϵ such that every point $x \in \mathcal{N}_\epsilon$ has a unique orthogonal projection onto Γ . Given a triangle $\mathbb{E}_h \in \mathcal{T}_h(\Gamma)$, we can directly extend the classical two-dimensional ‘‘flat’’ definitions characterizing proper triangulations. Thus, we denote the mesh parameter and mesh radius as $h = \max_{\mathbb{E} \in \mathcal{T}_h} h_{\mathbb{E}}$ and $r = \min_{\mathbb{E} \in \mathcal{T}_h} r_{\mathbb{E}}$, respectively, where $h_{\mathbb{E}}$ is the length of the longest edge of \mathbb{E}_h and $r_{\mathbb{E}}$ the radius of the circle inscribed in \mathbb{E}_h . Moreover, we assume that $\mathcal{T}_h(\Gamma)$ is shape-regular, i.e., there exists a strictly positive constant $\rho > 0$ independent of h such that:

$$\frac{r_{\mathbb{E}}}{h_{\mathbb{E}}} \geq \rho \quad \forall \mathbb{E}_h \in \mathcal{T}_h(\Gamma).$$

Remark 1. *As a consequence of the previous definitions, for any flat cell $\mathbb{E}_h \subset \Gamma_h$ there is a unique curved cell $\mathbb{E} \subset \Gamma$, and this correspondence is bijective. Hence, all the properties of $\mathcal{T}_h(\Gamma)$ are inherited by $\mathcal{T}(\Gamma)$ and can be given indifferently for only one of the two triangulations.*

Following the approach described in [2], the two dependent variables are defined in two different triangulations and two different functional spaces to avoid oscillations. This sort of inf-sup stability requirement is not yet fully understood and was used in both [1, 2] as a remedy for observed checkerboard-like oscillations. Thus, we employ the triangulation $\mathcal{T}_{h/2}(\Gamma)$ generated from $\mathcal{T}_h(\Gamma)$ by conformally refining each flat triangle. The new nodes in the conformal refinement are not moved back to the surface Γ to enhance the stabilization properties introduced by the refined mesh. The sub-triangles in the refined triangulation $\mathcal{T}_{h/2}$ are denoted by e_l while \mathbb{E}_r identifies triangles in $\mathcal{T}_h(\Gamma)$. We use $e_l \subset \mathbb{E}_r$ to denote those cells of $\mathcal{T}_{h/2}(\Gamma)$ that belong to \mathbb{E}_r .

Given a smooth function $\phi : \Gamma \rightarrow \mathbb{R}$, its smooth extension in \mathcal{N}_ϵ is well defined and is denoted by $\bar{\phi} : \mathcal{N}_\epsilon \rightarrow \mathbb{R}$. This smooth extension is used to define the tangential gradient of ϕ as follows:

Definition 1 (Tangential Gradient). *Let $\bar{\phi} : \mathcal{N}_\epsilon \rightarrow \mathbb{R}$ be the continuous extension of a smooth function $\phi : \Gamma \rightarrow \mathbb{R}$. The tangential gradient of ϕ at a point $x \in \Gamma$ is given by*

$$\nabla_{\Gamma} \phi(x) = \nabla \bar{\phi}(x) - \langle \nabla \bar{\phi}(x), \nu(x) \rangle \nu(x) = \mathbb{P}(x) \nabla \bar{\phi}(x), \quad (17)$$

is the unit oriented normal to the surface Γ at x , the projection tensor is given by $\mathbb{P}(x) = \mathbb{I} - \nu(x) \otimes \nu(x)$, the bilinear form $\langle \cdot, \cdot \rangle$ is the standard scalar product in \mathbb{R}^3 .

It turns out [28] that the tangential gradient is equivalent to the metric gradient (i.e. $\nabla_g \phi = \nabla_\Gamma \phi$) for any regular surface Γ . Moreover, Green's lemma holds for these tangential operators.

Then, we can define the SFEM DMK on Γ_h by simply employing the quantities defined in definition 1 and projecting (16) onto the finite dimensional FEM spaces $\mathcal{V}_h \subset H^1(\Gamma_h)$ and $\mathcal{W}_h \subset L^2(\Gamma_h)$. Note that $\nu_h = \nu(x)|_{\mathbb{E}}$ is constant on each triangle $\mathbb{E} \in \mathcal{T}_h(\Gamma_h)$, and so is $\mathbb{P}_h = \mathbb{I} - \nu_h \otimes \nu_h$. Thus it is convenient to use as test functions the Lagrange-polynomial basis functions of \mathcal{V}_h and \mathcal{W}_h , which are defined also triangle-wise. Then, the integrals over Γ_h transform into a sum over $\mathcal{T}_h(\Gamma_h) = \Gamma_h$, and we can write the following SFEM-DMK semi-discrete problem embedded in \mathbb{R}^3 :

Problem 3. Find $(\mu_h(t), u_h(t)) \in \mathcal{W}_h \times \mathcal{V}_h$ such that:

$$\int_{\Gamma_h} \mu_h(t) \langle \nabla_\Gamma u_h(t), \nabla_\Gamma \psi_i \rangle dx = \int_{\Gamma_h} (f^+ - f^-) \psi_i dx, \quad i = 1 \dots N, \quad (18a)$$

$$\int_{\Gamma_h} \partial_t \mu_h(t) \xi_s dx = \int_{\Gamma_h} \mu_h(t) (|\nabla_\Gamma u_h(t)| - 1) \xi_s dx, \quad s = 1, \dots, M, \quad (18b)$$

$$\int_{\Gamma_h} \mu(0) \xi_s dx = \int_{\Gamma_h} \mu_0 \xi_s dx, \quad s = 1, \dots, M, \quad (18c)$$

$$\int_{\Gamma_h} u_h \psi_i dx = 0 \quad i = 1, \dots, N, \quad (18d)$$

where $\mathcal{V}_h = \text{span}\{\psi_1, \dots, \psi_N\}$ and $\mathcal{W}_h = \text{span}\{\xi_1, \dots, \xi_M\}$.

Note that we have transformed the surface integrals into a sum of integrals on the planar triangles \mathbb{E} . Similarly, we can define the SFEM basis functions by means of standard (triangle-wise) three-dimensional Lagrange interpolating polynomials and project their Euclidean gradients onto each $\mathbb{E} \in \mathcal{T}_h(\Gamma_h)$ using \mathbb{P}_h .

Now we choose the same FEM spaces that worked in the planar case [2]. We denote by $\mathcal{P}_1(\mathbb{e})$ the set of affine functions supported on \mathbb{e} and with $\mathcal{P}_0(\mathbb{E})$ the set of constant functions supported on \mathbb{E} . Then we define $\mathcal{V}_h = \mathcal{P}_1(\mathcal{T}_{h/2}(\Gamma_h))$ and $\mathcal{W}_h = \mathcal{P}_0(\mathcal{T}_h(\Gamma_h))$, where

$$\begin{aligned} \mathcal{P}_1(\mathcal{T}_{h/2}(\Gamma_h)) &= \{v \in \mathcal{C}^0(\Gamma_h) : v|_{\mathbb{e}} \in \mathcal{P}_1(\mathbb{e}), \forall \mathbb{e} \in \mathcal{T}_{h/2}(\Gamma_h)\}, \\ \mathcal{P}_0(\mathcal{T}_h(\Gamma_h)) &= \{w : w|_{\mathbb{E}} \in \mathcal{P}_0(\mathbb{E}), \forall \mathbb{E} \in \mathcal{T}_h(\Gamma_h)\}. \end{aligned}$$

Using FEM terminology, we choose to approximate the transport density with non-conforming piecewise constant functions and the transport potential with conforming piecewise affine functions. Note that this choice is compatible with the dynamic (second) equation (18b) since $\nabla_\Gamma u_h|_{\mathbb{E}} \in \mathcal{P}_0(\mathbb{E})$ if $u_h|_{\mathbb{E}} \in \mathcal{P}_1(\mathbb{E})$. Now, separating the temporal and spatial variables, we can write the discrete transport density $\mu_h(t, x)$ and the discrete Kantorovich potential $u_h(t, x)$ and its tangential gradient as:

$$\begin{aligned} \mu_h(t, x) &= \sum_{r=1}^M \mu_r(t) \xi_r(x), & u_h(t, x) &= \sum_{j=1}^N u_j(t) \psi_j(x), \\ \nabla_\Gamma u_h(t, x) &= \sum_{j=1}^N u_j(t) \nabla_\Gamma \psi_j(x). \end{aligned}$$

We stress here that, by the way $\mathbb{e} \in \mathcal{T}_{h/2}(\Gamma_h)$ is built from $\mathbb{E} \in \mathcal{T}_h(\Gamma_h)$, \mathbb{E} is the union of four subcells \mathbb{e}_ℓ , i.e., using a local enumeration, $\mathbb{E} = \cup_{\ell=1}^4 \mathbb{e}_\ell$. Thus, the computation of the integral on the right-hand side of eq. (18b) on $\mathbb{E} \in \mathcal{T}_h(\Gamma_h)$ requires a simple arithmetic average of the gradients of the potential on the sub-triangles $\mathbb{e} \in \mathcal{T}_{h/2}(\Gamma_h)$:

$$\int_{\Gamma_h} \mu_h |\nabla_\Gamma u_h| \xi_s dx = \int_{\mathbb{E}_s} \mu_h |\nabla_\Gamma u_h| dx = \sum_{\ell=1}^4 \int_{\mathbb{e}_\ell} \mu_h |\nabla_\Gamma u_h| dx.$$

Denoting with $\boldsymbol{\mu}(t) = \{\mu_r(t)\}$ and $\mathbf{u}(t) = \{u_j(t)\}$ the curves describing the time evolution of the spatially projected finite-dimensional system, eq. (16) becomes:

$$\mathbf{A}[\boldsymbol{\mu}(t)] \mathbf{u}(t) = \mathbf{b}, \quad (19a)$$

$$\partial_t \boldsymbol{\mu}(t) = \mathbf{D}(\mathbf{u}(t)) \boldsymbol{\mu}(t), \quad \boldsymbol{\mu}(0) = \boldsymbol{\mu}_0, \quad (19b)$$

where the sparse stiffness matrix $\mathbf{A}(\boldsymbol{\mu}(t))$, and the diagonal matrix $\mathbf{D}(\mathbf{u}(t))$ are given by:

$$A_{i,j}(\boldsymbol{\mu}(t)) = \int_{\Gamma_h} \mu_h(t) \langle \nabla_{\Gamma} \psi_i, \nabla_{\Gamma} \psi_j \rangle dx \quad D_{r,r}(\mathbf{u}(t)) = \frac{1}{|\mathbb{E}_r|} \int_{\mathbb{E}_r} (|\nabla_{\Gamma} u_h(t, x)| - 1) dx.$$

The zero mean constraint on u_h is incorporated in the linear solution phase as detailed below.

3.2 Time discretization

The numerical solution of (19) is obtained by a forward Euler time discretization. This allows an easy resolution of the nonlinearities and an immediate decoupling of the resulting two algebraic systems of equations. Given a time sequence (t_k) , $k = 0, \dots, K_{\max}$ with $t_{k+1} = t_k + \Delta t_k$ we generate an approximating sequence (μ_h^k, u_h^k) defined as:

$$\begin{aligned} \mathbf{A}[\boldsymbol{\mu}^k] \mathbf{u}^k &= \mathbf{b}, \\ \boldsymbol{\mu}^{k+1} &= \boldsymbol{\mu}^k + \Delta t_k \mathbf{D}(\mathbf{u}^k) \boldsymbol{\mu}^k \end{aligned}$$

The first step involves the solution of a linear system whose matrix $\mathbf{A}[\boldsymbol{\mu}^k]$ is sparse and symmetric positive semidefinite. This is obtained by means of the preconditioned conjugate gradient algorithm using an IC(0)-based spectral preconditioner with selective updates, as proposed in [2, 38] and a deflation-like approach to incorporate the zero mean constraint. The second step involves the calculation of the cell gradients and a direct time update that exploits the diagonal structure of the system. At each time step, the step size Δt_k is calculated on the basis of the eigenvalues of matrix $\mathbf{D}(\mathbf{u}^k)$ to ensure stability of the forward Euler time-stepping.

Time-convergence is considered achieved by the discrete solution (μ_h^{k+1}, u_h^{k+1}) when the relative variation of μ_h is smaller than a given tolerance τ_T , i.e.,

$$\text{var}(\mu_h) := \frac{\|\mu_h^{k+1} - \mu_h^k\|_{L^1(\Gamma)}}{\Delta t_k \|\mu_h^k\|_{L^1(\Gamma)}} < \tau_T.$$

We indicate with t^* the time when equilibrium is numerically reached and with μ_h^* and u_h^* the corresponding μ_h^k and u_h^k .

3.3 Approximate solutions of the MK equations and Beckmann problem

The time-converged solutions μ_h^* and u_h^* are the approximations of the solutions to the MK equations μ^* and u^* . From these, we can calculate the approximate solution to Beckmann Problem given in eq. (13). Note that the gradient of $u_h(t)$ is defined on the refined triangles of $\mathcal{T}_{h/2}(\Gamma_h)$ while $\mu_h(t)$ is defined on the triangles of $\mathcal{T}_h(\Gamma_h)$. As done in the numerical solution algorithm, we project the gradient of $u_h(t)$ onto $\mathcal{T}_h(\Gamma_h)$ by simple averaging. Our approximate velocity $v_h(t) \in [\mathcal{P}_0(\mathcal{T}_h(M))]^3$ is then given by:

$$v_h(t)|_{\mathbb{E}_r} := \mu_h(t)|_{\mathbb{E}_r} \frac{1}{4} \sum_{\mathbb{e}_l \in \mathbb{E}_r} \nabla_{\Gamma} u_h(t)|_{\mathbb{e}_l} \quad (21)$$

We will denote v_h^* the velocity at the equilibrium time t^* .

In addition, we can calculate the Wasserstein-1 distance $W_1(f^+, f^-)$ between f^+ and f^- . According to Proposition 1, $W_1(f^+, f^-)$ corresponds to the minimum of the functional \mathcal{L}_g , which can be estimated as:

$$W_1^h(f^+, f^-) := \mathcal{L}_{g,h}(\mu_h^*) = \frac{1}{2} \int_{\Gamma_h} \mu_h^* |\nabla_{\Gamma} u_h^*|^2 dx + \frac{1}{2} \int_{\Gamma_h} \mu_h^* dx.$$

4 Numerical experiments

The test case devised for the verification of the temporal and spatial convergence properties of the scheme is settled on the unit sphere \mathcal{S}^2 . A constant density supported on a geodesic quadrilateral is rigidly moved from one position to another. In this case, the explicit formulas of the solution of the MK equations can be found. This allows us to test the accuracy of the proposed numerical scheme by computing the relative error in the approximation of the OT density, the optimal velocity field v^* solution of eq. (12), and the Wasserstein-1 distance. We also compare our numerical approximations with the ones obtained using the approach described in [25]. In this case, a quantitative comparison is done only in terms of accuracy, while we only report the CPU time required by our method because of the drastically different implementations of the companion software packages.

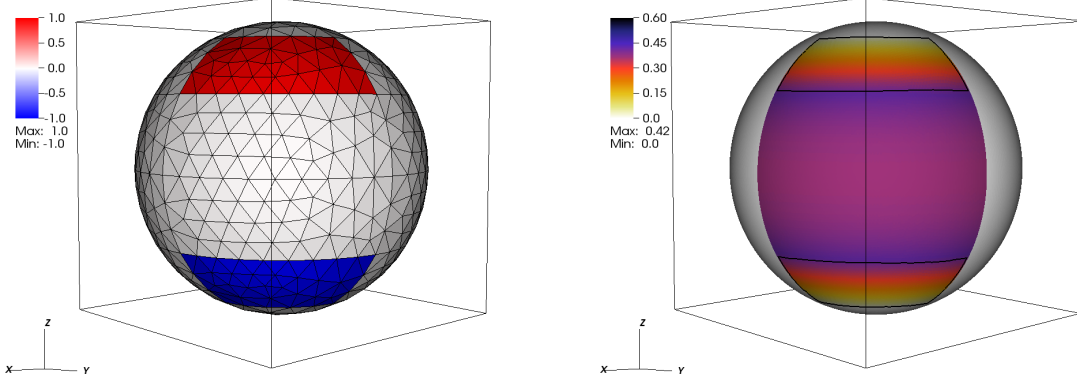


Figure 1: Spatial distribution of the L^2 -projection of $f^+ - f^-$ on the mesh \mathcal{T}_h with 554 nodes and 1104 triangles (left). Spatial distribution of the density μ^* together with the contour lines of the supports of f^+ and f^- (right).

4.1 Comparison with closed-form solutions

4.1.1 Description of the test case

The test case considers the unit sphere \mathcal{S}^2 equipped with the induced metric. The description of this test case is more easily carried out using polar coordinates (r, φ) defined with respect to the north pole $N = (0, 0, 1)$, where $r(x) = \text{dist}_g(x, N) \in]0, \pi[$ and $\varphi(x) \in]0, 2\pi[$ is the “longitude” angle. We consider two unit densities f^+ and f^- with supports given by:

$$\begin{aligned} \text{supp}(f^+) &= \{(r, \varphi) : [\pi/6 < r < \pi/3] \quad \varphi \in [0, \pi/2]\} \\ \text{supp}(f^-) &= \{(r, \varphi) : [2\pi/3 < r < 5\pi/6] \quad \varphi \in [0, \pi/2]\} . \end{aligned}$$

The approximate spatial distribution of f^+ and f^- is shown in Figure 1. For such densities, the pair (u^*, μ^*) solution of the MK equations eq. (10) is given by:

$$\tilde{\mu}^*(r, \varphi) = \begin{cases} (\cos(\pi/6) - \cos(r)) / \sin(r) & \text{if } \pi/6 < r < \pi/3 & 0 < \varphi < \pi/2 \\ (\cos(\pi/6) - \cos(\pi/3)) / \sin(r) & \text{if } \pi/3 < r < 2\pi/3 & 0 < \varphi < \pi/2 \\ (\cos(\pi/6) + \cos(r)) / \sin(r) & \text{if } 2\pi/3 < r < 5\pi/6 & 0 < \varphi < \pi/2 \\ 0 & \text{elsewhere} \end{cases}$$

$$\tilde{u}^*(r, \varphi) = -r$$

We obtained these explicit formulas adapting to \mathcal{S}^2 the exact solutions developed by [29] for the Euclidean MK equations. We recall that \tilde{u}^* represents only one possible solution of the MK equations, since in general the Kantorovich potential is unique up to constants within the support of μ^* , while outside it is not unique. The spatial distribution of μ^* is shown on the right panel of Figure 1. The explicit solution of Beckmann Problem can be derived using eq. (6), obtaining:

$$\tilde{v}^*(r, \varphi) = \tilde{\mu}^*(r, \varphi) \left(1 \cdot \frac{\partial}{\partial r}, 0 \cdot \frac{\partial}{\partial \varphi} \right), \quad (22)$$

where $\left(\frac{\partial}{\partial r}, \frac{\partial}{\partial \varphi} \right)$ are the coordinate vectors in $T_p \mathcal{S}^2$ with respect to the coordinate system (r, φ) .

We measure the accuracy of our numerical approximation by calculating the error in the solution of Beckmann problem \tilde{v}^* and the error in the evaluation of the Wasserstein-1 distance $W_1(f^+, f^-)$. The former is evaluated as:

$$\text{err}_{BP}(v_h^*) := \frac{\int_{\Gamma_h} |v_h^* - v^*| dV_g}{\int_{\mathcal{S}^2} |v^*| dV_g} .$$

where the integral in the numerator is approximated via the mid-point rule on Γ_h . The use of the above error definition allows the evaluation of the accuracy on both the velocity direction $\nabla_{\Gamma} \tilde{u}^*$ and magnitude given by $\tilde{\mu}^*$. Moreover, it is

consistent with the application of the approach proposed in [25] and thus it allows a fair comparison with published results.

The error in the Wasserstein-1 distance between f^+ and f^- deserves a specific evaluation because of its importance in applications. We then define:

$$\text{err}_{W_1}(W_1^h) := \frac{|W_1^h(f^+, f^-) - W_1(f^+, f^-)|}{W_1(f^+, f^-)},$$

where W_1^h denotes the specific numerical approximation of the Wasserstein-1 distance. For the test case considered, the exact value can be calculated as:

$$W_1(f^+, f^-) = \int_{S^2} \mu^* = \left(\frac{\pi\sqrt{3}}{6} - (\sqrt{3} - 1) \left(2 - \frac{\pi}{3} \right) \right) \frac{\pi}{4} \approx 0.876739625901484.$$

Finally, we report a brief description of the implementation of the EMDADMM approach proposed by [25], which is our benchmark against which we compare our method. In EMDADMM, the approximate solution \bar{v}_h is obtained as the following linear combination:

$$\bar{v}_h(x) = \nabla_g \bar{u}(x) + \sum_i^{N_e} c_i V_i(x)$$

where \bar{u} solves the Poisson equation $-\Delta_g \bar{u} = f^+ - f^-$, while $V_i(x)$ are vector fields built from the piecewise linear approximation of the the first N_e eigenfunctions of the Laplace Beltrami operator (i.e., eigenvector of the corresponding FEM stiffness matrix). The optimal coefficient vector c is found by means of the Alternating Direction Method of Multipliers (ADMM) [39]. In our tests we used the suggested value $N_e = N_h/16$, where N_h is the number of nodes in \mathcal{T}_h .

In our experiments, S^2 is approximated by an initial triangulation ($\mathcal{S}_h^2 = \Gamma_h = \mathcal{T}_h(S^2)$) made up of 554 nodes and 1124 triangles (reported in Figure 1) obtained using the software described in [40]. This initial triangulation is constrained to have nodes lying exactly on the meridians and parallels defining the boundaries of $\text{supp}(f^+)$ and $\text{supp}(f^-)$. Successive uniform refinements of the initial mesh Γ_h are obtained by calculating edge mid-points and moving them to the unit sphere surface, taking care of preserving the alignment with $\text{supp}(f^+)$ and $\text{supp}(f^-)$. This process is repeated three times, for a total of four mesh levels. At each refinement level, the sub-grid $\mathcal{T}_{h/2}(S^2)$ is obtained by uniform refinement with edge midpoints maintained in the original planar triangle and not moved to the surface.

4.1.2 Experimental results

Convergence of Surface DMK. The experimental convergence results for the surface DMK are summarized in Figure 2. Denoting with $\mu_h(t)$ the piecewise linear interpolation of the sequence μ_h^k , each row of Figure 2 show the time evolution of the quantities $\text{var}(\mu_h(t))$, $\text{err}_{BP}(v_h^*(t))$, and $\text{err}_{W_1}(\mu_h(t))$. Each plot contains the results obtained for the four considered refinement levels. To better envision the computational effort of our approach, the right panels report the same quantities with respect to the CPU time $t_{CPU}(t)$, i.e., the CPU time in seconds to arrive at simulation time t on a first-generation 2.2GHz Intel-I5 (1-core) laptop computer.

The top-left panel in Figure 2 shows a monotone convergence toward equilibrium for all refinement levels. The same monotonically decreasing profile is observed in the $\text{err}_{BP}(v_h(t))$ plots. Here the error saturates at a level that decreases by a constant factor at every refinement, indicating the achievement of the spatial resolution limit attainable with the given triangulation. In addition, these results suggest first order convergence of the spatial discretization for the solution of Beckmann problem. Finally, the bottom panels show the evolution of the relative error on the Wasserstein-1 distance. The non-monotone profiles can be explained as follows. First of all, note that the Wasserstein-1 distance is evaluated as the minimum of \mathcal{L}_g , and thus we are approximating W_1 from above. On the other hand, the integrals are approximated by the mid-point quadrature rule from below (the area of the linear triangles is always smaller or equal than that of the corresponding surface triangle). At a certain time \hat{t} , the overestimation of \mathcal{L}_g and the underestimation of the integrals compensate and $\text{err}_{W_1}(\mu_h(\hat{t}))$ becomes artificially close to zero. After \hat{t} , the error in the approximation of the integral dominates and the global error saturates at a value that depends on the mesh size h .

Figure 3 shows the experimental mesh convergence attained by the surface DMK and the EMDADMM methods on the solution of the L^1 -OTP in terms of the velocity field of Beckmann problem ($\text{err}_{BP}(v_h^*)$, left panel) and the calculation of the Wasserstein-1 distance ($\text{err}_{W_1}(\mu_h^*)$, right panel). Four nested mesh refinements are used and the convergence lines (in log-log plot) are calculated by linear least squares. In the first case the DMK achieves a rate of order one,

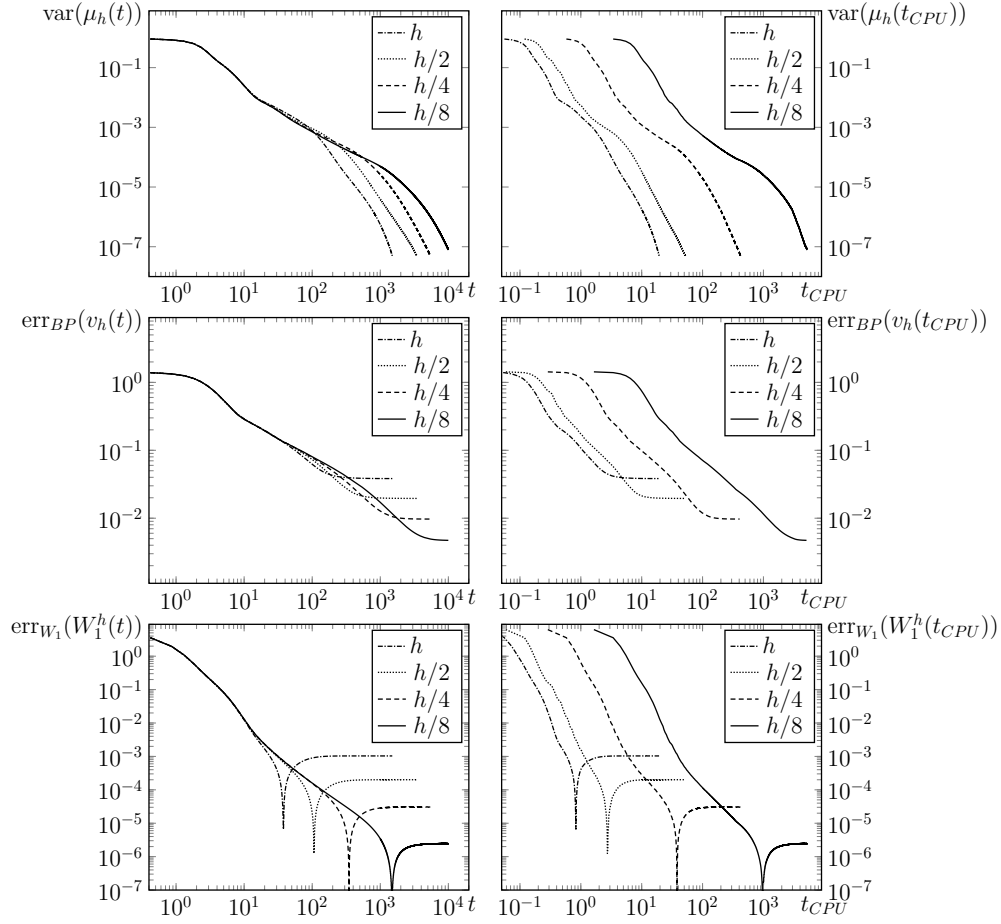


Figure 2: Experimental convergence towards the MK solution. Left column: time (t) evolution of $\text{var}(\mu_h(t))$, which measures convergence towards equilibrium, and of $\text{err}(v_h(t))$ and $\text{err}_{W_1}(\mu_h(t))$, which measure the accuracy of the spatial approximation. The results are obtained on successive uniform refinements of a an initial mesh with 554 nodes and 1124 triangles. Right column: values of the four simulation metrics as a function of computational time (t_{CPU} , seconds). The simulations were conducted on a first-generation 2.2GHz Intel-I5 (1-core) laptop computer.

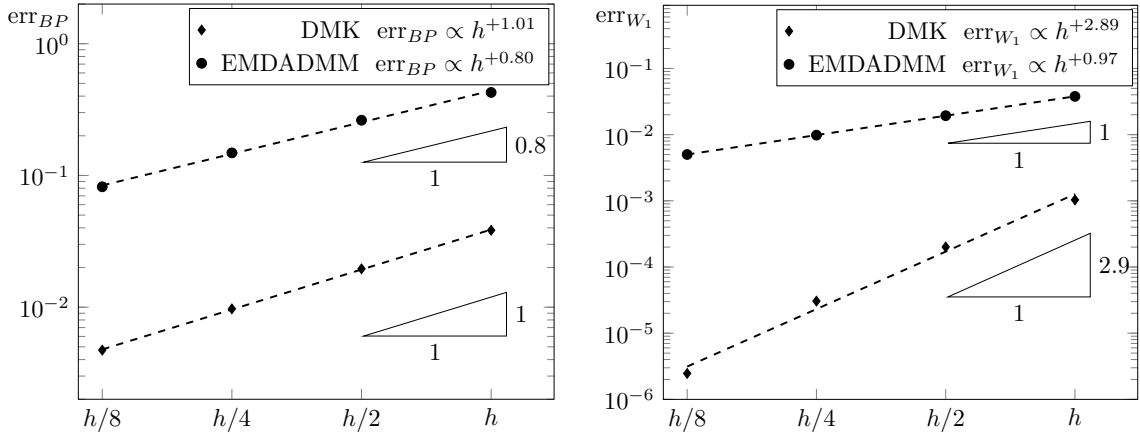


Figure 3: Spatial convergence of DMK and EMDADMM on the relative Beckmann error $\text{err}_{BP}(v_h^*)$ (left) and on the Wasserstein-1 distance $\text{err}_{W_1}(\mu_h^*)$ (right). The errors are calculated on four mesh refinements and the corresponding experimental spatial convergence rate with respect to mesh parameter h , evaluated by linear approximation, is reported in the plot legend.

coherent with the piecewise constant (\mathcal{P}_1) discretization of the transport density and of the gradient of the Kantorovich potential. This result is also consistent with the results presented for the Euclidean case in [2]. The experiments with the EMDADMM method show a slight sub-optimal rate of convergence of about 0.8, providing a further indication of the lower accuracy of this scheme with respect to DMK. The right panel of Figure 3 shows the convergence plots when the two schemes are applied for the calculation of the W_1 distance. The experimental error obtained with DMK scales almost cubically with the mesh parameter h , while EMDADMM maintains first order convergence.

The accuracy attained by the DMK approach is much higher than the one attained by the EMDADMM method. Already at the coarsest triangulation the DMK accuracy is well below 0.1% with a CPU time of approximately 2 seconds. In contrast, EMDADMM with a comparable computational effort, achieves on the the same mesh an accuracy of about 4%.

5 Conclusion

We propose the numerical solution of the L^1 -OT problem on triangulated surfaces via the DMK approach, and the calculation of the Wasserstein-1 distance. From the computational point of view, besides the totally inexpensive projection for the gradient of basis functions $\mathcal{P}_1(\mathcal{T}_{h/2})$, finding the approximating optimal solution (μ_h^*, u_h^*) on surfaces requires the same effort as on the 2d Euclidean setting. A number of improvements (multilevel approximation, hardware acceleration, or implicit time-stepping scheme solved via Newton-Raphson, like in [41]) can be considered to improve the computational efficiency of the scheme but in this paper we are more interested in testing the accuracy of the method applied to surfaces. In the test case where an exact solution of the MK equations is known, the experimental convergence rate in the approximation of the solution of the L^1 -OT problem is shown to be linear with respect to the mesh parameter h . However, the experimental rate of convergence in the computation of the Wasserstein-1 distance showed superconvergence that has not yet been explained. In fact, we found an almost cubic order of convergence and in general the discrete DMK approach showed noticeably better accuracy and performance with respect to existing algorithms.

References

- [1] Enrico Facca, Franco Cardin, and Mario Putti. Towards a stationary Monge–Kantorovich dynamics: The physarum polycephalum experience. *SIAM J. Appl. Math.*, 78(2):651–676, 2018.
- [2] Enrico Facca, Sara Daneri, Franco Cardin, and Mario Putti. Numerical solution of Monge–Kantorovich equations via a dynamic formulation. *J. Scient. Comput.*, 82(3):1–26, 2020.
- [3] Gaspard Monge. *Mémoire sur la théorie des déblais et des remblais*. De l’Imprimerie Royale, 1781.
- [4] Leonid V. Kantorovich. On the translocation of masses. *Management Sci.*, 5:1–4, 1958.
- [5] Luigi Ambrosio. Lecture notes on optimal transport problems. In *Lecture Notes in Mathematics*, pages 1–52. Springer, Berlin, Heidelberg, 2003.
- [6] Cédric Villani. *Topics in optimal transportation*. Number 58 in Graduate studies in mathematics. American Mathematical Soc., 2003.
- [7] Cédric Villani. *Optimal Transport: Old and New*, volume 338. Springer Science & Business Media, 2008.
- [8] Filippo Santambrogio. *Optimal Transport for Applied Mathematicians*. Birkäuser, NY, 2015.
- [9] Jean-David Benamou and Yann Brenier. A computational fluid mechanics solution to the Monge-Kantorovich mass transfer problem. *Numer. Math.*, 84(3):375–393, 2000.
- [10] Jean-David Benamou, Yann Brenier, and K Guittet. The Monge–Kantorovich mass transfer and its computational fluid mechanics formulation. *Int. J. Numer. Methods Fluids*, 40(1-2):21–30, September 2002.
- [11] Ishaan Gulrajani, Faruk Ahmed, Martin Arjovsky, Vincent Dumoulin, and Aaron C Courville. Improved training of Wasserstein gans. In *Adv. Neural Inf. Process. Syst.*, pages 5767–5777. Curran Associates, Inc., 2017.
- [12] Yongxin Chen, Tryphon T. Georgiou, and Michele Pavon. Optimal transport over a linear dynamical system. *IEEE T. Automat. Contr.*, 62(5):2137–2152, 2017.
- [13] G L Delzanno, L Chacón, J M Finn, Y Chung, and G Lapenta. An optimal robust equidistribution method for two-dimensional grid adaptation based on Monge–Kantorovich optimization. *J. Comp. Phys.*, 227(23):9841–9864, December 2008.
- [14] Ludovic Métivier, Romain Brossier, Quentin Merigot, E Oudet, and Jean Virieux. An optimal transport approach for seismic tomography: Application to 3d full waveform inversion. *Inverse Probl.*, 32(11):115008, 2016.

- [15] Justin Solomon, Fernando De Goes, Gabriel Peyré, Marco Cuturi, Adrian Butscher, Andy Nguyen, Tao Du, and Leonidas Guibas. Convolutional Wasserstein distances: Efficient optimal transportation on geometric domains. *ACM Trans. Graph.*, 34(4):66, 2015.
- [16] Gabriel Peyré and Marco Cuturi. Computational optimal transport. *Found. Trends Mach. Learn.*, 11(5-6):1–257, January 2019.
- [17] Jean-David Benamou and Guillaume Carlier. Augmented Lagrangian methods for transport optimization, mean field games and degenerate elliptic equations. *J. Opt. Theory Appl.*, 167(1):1–26, 2015.
- [18] Wuchen Li, Ernest Ryu, Stanley Osher, Wotao Yin, and Wilfrid Gangbo. A parallel method for earth mover’s distance. *J. Scient. Comput.*, 08 2017.
- [19] Marco Cuturi. Sinkhorn distances: Lightspeed computation of optimal transport. In *Advances in neural information processing systems*, pages 2292–2300, 2013.
- [20] Aude Genevay, Marco Cuturi, Gabriel Peyré, and Francis Bach. Stochastic optimization for large-scale optimal transport. In D. Lee, M. Sugiyama, U. Luxburg, I. Guyon, and R. Garnett, editors, *Advances in Neural Information Processing Systems*, volume 29, pages 3440–3448. Curran Associates, Inc., 2016.
- [21] Lawrence C Evans and Wilfrid Gangbo. *Differential equations methods for the Monge–Kantorovich mass transfer problem*, volume 653. American Mathematical Soc., 1999.
- [22] Enrico Facca and Federico Piazzon. Transport energy. ArXiv preprint available, 2019.
- [23] Mikhail Feldman and Robert J. McCann. Monge’s transport problem on a riemannian manifold. *Trans. Amer. Math. Soc.*, 354(4):1667–1697, 2001.
- [24] Aldo Pratelli. Equivalence between some definitions for the optimal mass transport problem and for the transport density on manifolds. *Ann. di Mat. Pura ed Appl.*, 184:215–238, 06 2005.
- [25] Justin Solomon, Raif Rustamov, Leonidas Guibas, and Adrian Butscher. Earth mover’s distances on discrete surfaces. *ACM Trans. Graph.*, 33(4):67:1–67:12, July 2014.
- [26] Zhengyu Su, Wei Zeng, Yalin Wang, Zhong-Lin Lu, and Xianfeng Gu. Shape classification using Wasserstein distance for brain morphometry analysis. In *International Conference on Information Processing in Medical Imaging*, pages 411–423. Springer, 2015.
- [27] Hugo Lavenant, Sebastian Clatici, Edward Chien, and Justin Solomon. Dynamical optimal transport on discrete surfaces. *ACM Trans. Graph.*, 37(6):1–16, January 2019.
- [28] Gerhard Dziuk and Charles M Elliott. Finite element methods for surface pdes. *Acta Num.*, 22:289–396, 2013.
- [29] Giuseppe Buttazzo and Eugene Stepanov. On regularity of transport density in the Monge–Kantorovich problem. *SIAM J. Control Optim.*, 42(3):1044–1055, 2003.
- [30] Guy Bouchitté and Giuseppe Buttazzo. Characterization of optimal shapes and masses through Monge–Kantorovich equation. *J. Eur. Math. Soc.*, 3(2):139–168, 2001.
- [31] Guy Bouchitté, Giuseppe Buttazzo, and Pierre Seppecher. Energies with respect to a measure and applications to low dimensional structures. *Calc. Var. Partial Diff. Equ.*, 5(1):37–54, 1996.
- [32] Ilaria Fragalà and Carlo Mantegazza. On some notions of tangent space to a measure. *R. Soc. Edinburgh - Proc.*, 129(2):331–342, 1999.
- [33] Mikhail Feldman and Robert J. McCann. Uniqueness and transport density in monge’s mass transportation problem. *Calc. Var. Partial Diff. Equ.*, 15(1):81–113, 2002.
- [34] Luigi De Pascale, Lawrence C Evans, and Aldo Pratelli. Integral estimates for transport densities. *Bull. London Mat. Soc.*, 36(3):383–395, 2004.
- [35] Filippo Santambrogio. Absolute continuity and summability of transport densities: simpler proofs and new estimates. *Calc. Var. Partial Diff. Equ.*, 36(3):343–354, 2009.
- [36] Luigi Ambrosio, Nicola Gigli, and Gisueppe Savare. *Gradient Flows: In Metric Spaces and in the Space of Probability Measures*. Lectures in Mathematics. ETH Zürich. Birkhäuser Basel, 2005.
- [37] Jean-Marie Morvan. *Generalized Curvatures*, volume 2 of *Geometry and Computing*. Springer Science & Business Media, Berlin, Heidelberg, May 2008.
- [38] Luca Bergamaschi, Enrico Facca, Ángeles Martínez Calomardo, and Mario Putti. Spectral preconditioners for the efficient numerical solution of a continuous branched transport model. *J. Comput. Appl. Math.*, 354:259–270, 2018.

- [39] Stephen Boyd. Distributed optimization and statistical learning via the alternating direction method of multipliers. *Found. Trends Mach. Learn.*, 3(1):1–122, 2011.
- [40] Per-Olof Persson and Gilbert Strang. A simple mesh generator in Matlab. *SIAM Rev.*, 46(2):329–345, 2004.
- [41] Enrico Facca and Michele Benzi. Fast iterative solution of the optimal transport problem on graphs. *SIAM J. Sci. Comput.*, 2021. To appear, ArXiv preprint available.